



Technical report

## Duplex electroless Ni-P/Ni-Cu-P coatings: Preparation, evaluation of microhardness, friction, wear, and corrosion performance

Palash Biswas, Suman Kalyan Das and Prasanta Sahoo 

Department of Mechanical Engineering, Jadavpur University, Kolkata-700 032, India

Corresponding author:  [prasanta.sahoo@jadavpuruniversity.in](mailto:prasanta.sahoo@jadavpuruniversity.in); Tel.: +91-33-2457-2660

Received: May 30, 2022; Accepted: September 14, 2022; Published: October 23, 2022

### Abstract

The current study focuses on the development of duplex Ni-P/Ni-Cu-P coatings by the electroless deposition method. Coatings are developed on mild steel substrates with Ni-Cu-P as the outer layer and Ni-P as the inner layer and vice versa. The coated samples are heat-treated at temperatures ranging between 200 to 800 °C during 1 and 4 h. Coated samples are characterized by scanning electron microscopy (SEM), energy-dispersive X-ray spectroscopy (EDS) and X-ray diffraction (XRD). The effect of heat treatment temperature and its time duration on the hardness, friction and wear behaviour of both coatings are evaluated and compared. This would help in understanding how heat treatment influences the duplex system of coatings and helps in identifying the suitable condition of heat treatment for optimal performance of the coating. It is observed that heat treatment has a positive influence over the coating performance, which is the best when treated under optimal temperature and time duration conditions. The corrosion behaviour of the coatings is also assessed with the help of electrochemical techniques, viz. potentiodynamic polarization and electrochemical impedance spectroscopy. The results show that the duplex coatings can provide substantial protection to the mild steel substrates. Heat treatment is also found to have a significant influence on the corrosion behaviour of duplex coatings.

### Keywords

Mild steel; electroless nickel deposits; duplex coatings; heat treatment; physical properties; corrosion

### Introduction

Electroless deposited nickel (EN) coating enhances corrosion and wear resistance, leaving a consistent, homogeneous nickel coating for high-precision products [1]. The coating may be applied to ferrous and nonferrous surfaces of any geometry or complicated shape. For these reasons, EN coatings are gaining popularity across various industrial applications. EN coating was originally invented in 1946 by Brenner and Riddell [2]. No electricity is required in this process and the coating happens due to an autocatalytic reduction process [3]. This enables a greater range of industrial

parts, such as electrical/mechanical tools, driveshafts, valve pumps, oil field valves, and engineering equipment, to be surface finished with this coating [4-6]. In fact, electroless nickel deposits are found to be bio-compatible, offering resistance against bacterial growth [7].

Electroless deposited Ni-P coating is less porous than electrodeposited coating and protects substrates, *viz.* steel, from corrosion. It is gentle in application since it can be administered with zero or little compressive stress. Electroless plating is generally considered a more efficient, precise, and cost-effective coating technique.

There is some similarity between electroless deposition and the nitriding process. Nitriding is a thermochemical technique where the surface of the steel substrate is diffused with nascent nitrogen in order to enhance the surface hardness of the substrate. It does not require the substrate to undergo any phase transformation and in fact, there is not much dimensional change and no post-processing is involved [8]. Electroless Ni-P can also produce a stronger, higher-quality finish with less equipment than the electrodeposition method. For these aspects, Ni-P coating is used to offer abrasion and wear resistance, corrosion resistance, and hardness to parts in a variety of circumstances. It is widely applied in aerospace, construction, electronics, engineering, oil and gas, and various other industries [9,10]. The electroless deposited Ni-P alloy coating is supersaturated in the as-deposited condition and can be reinforced by the precipitation of nickel phosphide ( $\text{Ni}_3\text{P}$ ) crystallites with appropriate heat treatment. Electroless Ni-P coating is reported to offer enhanced hardness and tribo-corrosion performance to aluminium alloys [11].

The ternary alloy coating, which adds a third element to the binary Ni-P system, is a mode for obtaining customized deposit properties. The ternary Ni-X-P alloy, in which X is often a transition metal like W, Co, Mn, Cu, Re, and Mo, often has better characteristics than the binary Ni-P alloy and hence has a wider range of applicability [12-15]. Copper incorporation within the Ni-P alloy coating may improve thermal stability, paramagnetic stability, anti-corrosion capability, and aesthetic aspects. Ni-Cu-P coating is better than Ni-P coating in many aspects [16]. Increasing Cu content in the Ni-P matrix improved corrosion resistance, a slower deposition rate, and finer-grained deposits [17].

The incorporation of nanoparticles giving rise to nanocomposite coatings is found to have a lot of applications [18]. To further improve mechanical, physical, tribological, and anti-corrosion properties of the coating, researchers have recently shifted their attention to developing duplex [19-22], graded [23], and multilayer coatings [24-25]. Ni-P/Ni-B duplex systems achieve superior hardness compared to individual layers and provide good protection to high-velocity oxygen fuel-sprayed stainless steel substrates [22]. This duplex system also offers higher tribo-corrosion performance to AA7075 aluminium alloy [26].

The present work aims to develop duplex electroless Ni-P/Ni-Cu-P coating with Ni-Cu-P as the outer layer in the first set and Ni-P as the outer layer in the second set of experiments. The impact of various heat treatment conditions on the performance of these duplex coatings is investigated and compared. The coatings are heat-treated for 1 and 4h, respectively, at temperatures ranging from 400 to 800 °C. Microstructure characterization is carried out with the help of a scanning electron microscope (SEM). The phase transformation and chemical composition performance of the duplex coating are studied using X-ray diffraction analysis (XRD) and energy dispersive X-ray analysis (EDX), respectively. Dry-sliding wear test of the duplex-coated samples is conducted in a pin-on-disc tribometer. Potentiodynamic polarization (PP) and electrochemical impedance spectroscopy (EIS) are used to evaluate the corrosion behaviour of the duplex set of coatings.

## Experimental

### *Duplex Ni-P/Ni-Cu-P coating deposition*

Electroless deposition of duplex Ni-P/Ni-Cu-P coating was carried out on AISI 1040 low-carbon steel. The substrates were prepared according to the following dimensions - pin samples  $\phi 6 \times 30$  mm and square samples  $15 \times 15 \times 2$  mm. As surface interactions are dependent on the shape of the contacting surfaces [27], all substrates were ground to about the same roughness value. Steel samples were carefully cleaned with deionized water and running water. After rinsing, the samples were degreased with acetone, and the final wash was made with distilled water. After that, the samples were submerged in 50 % HCl solution for 2 minutes and washed in distilled water. Then, the substrates were activated by immersing in a heated (55 °C) solution of palladium chloride and HCl for about 15 seconds. This step was included to increase the initial coating deposition rate. For the deposition of the first set of duplex systems, the samples were firstly immersed in an electroless Ni-P bath for the inner layer of deposition. Ni-P bath composition and deposition conditions are given in Table 1 [28].

**Table 1.** Composition of Ni-P bath

Component	Concentration, g l <sup>-1</sup>
Nickel -chloride	20
Nickel- sulphate	20
Sodium- hypophosphite	24
Sodium- succinate	12
Condition	
Temperature, °C	82±2
pH	4.5-5.5

For Ni-P coatings, a combination of nickel chloride (NiCl<sub>2</sub>·6H<sub>2</sub>O) and nickel sulfate (NiSO<sub>4</sub>·6H<sub>2</sub>O) is taken as the source of nickel. While in the case of Ni-Cu-P coatings, the source of nickel and copper were nickel-sulfate (NiSO<sub>4</sub>·6H<sub>2</sub>O) and copper sulfate pentahydrate (CuSO<sub>4</sub>·5H<sub>2</sub>O), respectively. Sodium hypophosphite (NaPO<sub>2</sub>H<sub>2</sub>) was used as the reducing agent for both coatings. For the outer layer of deposition, the samples were dipped in electroless Ni-Cu-P solution after completion of the specified time duration. Ni-Cu-P bath composition and deposition conditions are stated in Table 2 [29]. The dual bath technique is used to deposit two successive layers of Ni-P (inner) and Ni-Cu-P (outer) over the substrates giving rise to duplex Ni-P/Ni-Cu-P coatings. The samples were removed from the bath after 4 hours of deposition, washed in deionized water, and dried.

**Table 2.** Composition of Ni-Cu-P bath

Component	Concentration, g l <sup>-1</sup>
Nickel- sulphate	25.0
Trisodium citrate dihydrate	45.0
Sodium- hypophosphite	25.0
Copper sulphate pentahydrate	12.0
Condition	
Temperature, °C	90±2
pH	7.0 – 8.0

In a similar manner, a duplex Ni-Cu-P/Ni-P (Ni-Cu-P as the inner layer and Ni-P as the outer layer of deposition) system is deposited. The deposition time was fixed at 2 hours for each layer of deposition for both sets of experiments. For easy reference throughout the text, the nomenclature presented in Table 3 will be followed.

**Table 3.** Nomenclature of coatings

Coating set	Nomenclature
Ni-P/Ni-Cu-P (Ni-P inner layer and Ni-Cu-P outer layer)	Coating-1
Ni-Cu-P/Ni-P (Ni-Cu-P inner layer and Ni-P outer layer)	Coating-2

### Heat treatment of duplex coating

The various properties of EN coatings, viz. phase structure, morphology, etc., are influenced by the heat treatment process. Above a specific heat treatment temperature, electroless nickel coatings are observed to change phase (from amorphous to crystalline). After this phase transformation, the hardness value is increased, and the wear rate of EN coatings is reduced. Duplex electroless nickel-plated samples were heated in a muffle furnace (Electro Scientific Equipment, Howrah-India) at temperatures ranging from 200 to 800 °C for time durations of 1 and 4 h. The reason for selecting 4 h as heat treatment duration is to observe the effect of long-duration heat treatment on the coating microstructure and performance. The samples are removed from the muffle furnace after the completion of heat treatment and air-cooled to room temperature.

### Microhardness measurement

The microhardness of the duplex coatings is measured by a Vickers microhardness tester (Model-VMHT MOT, Technische Mikroskopie) in both as-deposited and heat-treated conditions. The following parameters are maintained: a constant load of 100 gf, speed of 25  $\mu\text{m s}^{-1}$ , and dwell time of 15 s. On each sample, three readings were recorded, and the average value was reported. The hardness of the samples was determined by the diagonal length of the square indent. A low amplification optical magnifying equipment part of the hardness tester was used to measure this length.

### Morphology, composition analysis and phase structure analysis

Field emission scanning electron microscopy (FESEM) is used to obtain a high-resolution image of the surface morphology of the duplex coatings. The equipment used is FEI Quanta Carl Zeiss, Model No. EVO LS 10 (Everhart-Thornley Secondary Electron Detector). An energy dispersive X-ray (EDX) analyser under high vacuum at 20 kV is employed to obtain systematic observation of coating composition.

The phase structure of the coating was examined using the X-ray diffraction (XRD) technique (Rigaku, Ultima III). Scanning is done at a diffraction angle ( $2\theta$ ) ranging from 20 to 80° based on the available literature [30]. The following parameters were used to measure phase structure: scan width of 0.02° and scanning speed of 1.0°  $\text{min}^{-1}$ . The sharp peak in the case of XRD plots represents the crystalline phase, while diffused peak indicates the amorphous phase [31].

### Tribological test

The tribological behavior of both the duplex coatings in the as-deposited and heat-treated states are carried out on a pin-on-disc tribometer (TR-20LE-CHM-400, Ducom, India) at ambient condition (25 °C) in a dry state. The duplex-coated pin samples were fixed and aligned with a revolving counterface disc of hardened EN 31 (58- 62HRC) steel. In comparison to the coated samples, the counterface disc material shows negligible wear. Tribological tests were performed with a constant speed of 50 RPM, a normal load of 20 N, and a sliding distance of 94.2 m [28]. Also, the sliding duration was fixed at 10 min, and the track diameter of 60 mm was maintained. The responses considered were: wear in terms of mass loss and coefficient of friction (COF). A precision weighing machine with a reading of 0.01 mg was used to measure the mass loss of the duplex coatings immediately after the tribo-test. The frictional force was recorded by a button-type load cell with a

capacity of 10 kg and a precision of  $0.1 \pm 1$  % of the measured force. The density of the EN coating is considered  $8.0 \text{ g cm}^{-3}$ .

### *Corrosion test*

An electrochemical corrosion test was performed in a 3.5 wt.% NaCl solution to assess the corrosion resistance of the present set of coatings. The resulting Tafel curve and impedance charts (ACM Instruments GILL AC, UK) were constructed. Nyquist plots were obtained through electrochemical impedance spectroscopy. The tests were carried out using a standard three-electrode configuration. A saturated calomel electrode was used as the reference electrode as it provides a stable potential. The sample under consideration was the working electrode, and a platinum electrode was taken as a counter electrode. The contact area with NaCl solution for all samples was kept constant at  $1 \text{ cm}^2$ . In the test, the frequency range was kept between 10 kHz to 0.01 Hz and the ac signal amplitude was at 32 mV RMS. During the potentiodynamic test, the scanning rate was maintained at  $1 \text{ mV s}^{-1}$  [32]. Starting and inverse potentials were considered as -250 and +250 mV, respectively.

## **Results and discussion**

### *Microstructure characterization and composition analysis (EDX)*

The FESEM micrographs of as-plated and heat-treated Coating-1 are shown in Figure 1. The heat treatment temperature and the amount of phosphorous content influence the phase structure of the coatings [33], leading to changes in its surface morphology. The as-plated coating reveals a cauliflower-like morphology, as seen in Figure 1a, which is also reported by several researchers [4,9]. The average size of the nodule is found to be around  $5 \mu\text{m}$ . Almost no visible pores imply that the formed coating is highly dense. The heat treatment effect is observed prominently in the microstructure. After heat treatment of the duplex coating, the size of the nodules grows larger (Figure 1b-f). At  $600 \text{ }^\circ\text{C}$  temperature with 1 h duration, the nodule is found to be flattening. In fact, the inflated is more prominent for increasing heat treatment temperature and prolonged duration of heating. At  $800 \text{ }^\circ\text{C}$  temperature with 1 h duration, the surface of the coating develops a few cracks, which may be due to the relief of accumulated thermal stress, which is also reported in previous work [28]. Furthermore, at high temperatures (at  $600$  or  $800 \text{ }^\circ\text{C}$ ), few dark spots are observed on the surface. This may indicate the formation of oxide phases on the samples. The coating thickness is obtained around  $40 \mu\text{m}$  as observed from cross-cut samples.

In the case of Coating-2, as-deposited coating reveals a similar globular structure (Figure 2a). However, the globules are more prominent compared to Coating-1 morphology. The effect of heat treatment is prominently observed in microstructure, *i.e.*, the size of the nodule increases (Figure 2b-f). At higher temperatures ( $600$  or  $800 \text{ }^\circ\text{C}$ ) and prolonged time duration (1 and 4 h), the smoothness on the surface of the nodules is lost and some pores are visible (Figure 2e). The porosity of the coating seems to be increased for high temperatures reported in one of the previous studies [34].

The elemental composition of the coatings was determined using EDX and displayed in Figure 3. For both coatings, the phosphorous content indicates that the coatings belong to the high phosphorous category. The high phosphorus content in the duplex coating indicates its amorphous nature, as reported in the literature [4,35].

Additionally, line EDX (Figure 4) is conducted along the coating cross-section to get an idea about the variation of the coating composition. From Figure 4, it is found that the duplex system of coatings is more or less successfully developed. This is mainly inferred from the marked variation in wt. % of copper near the middle of the combined deposit thickness.

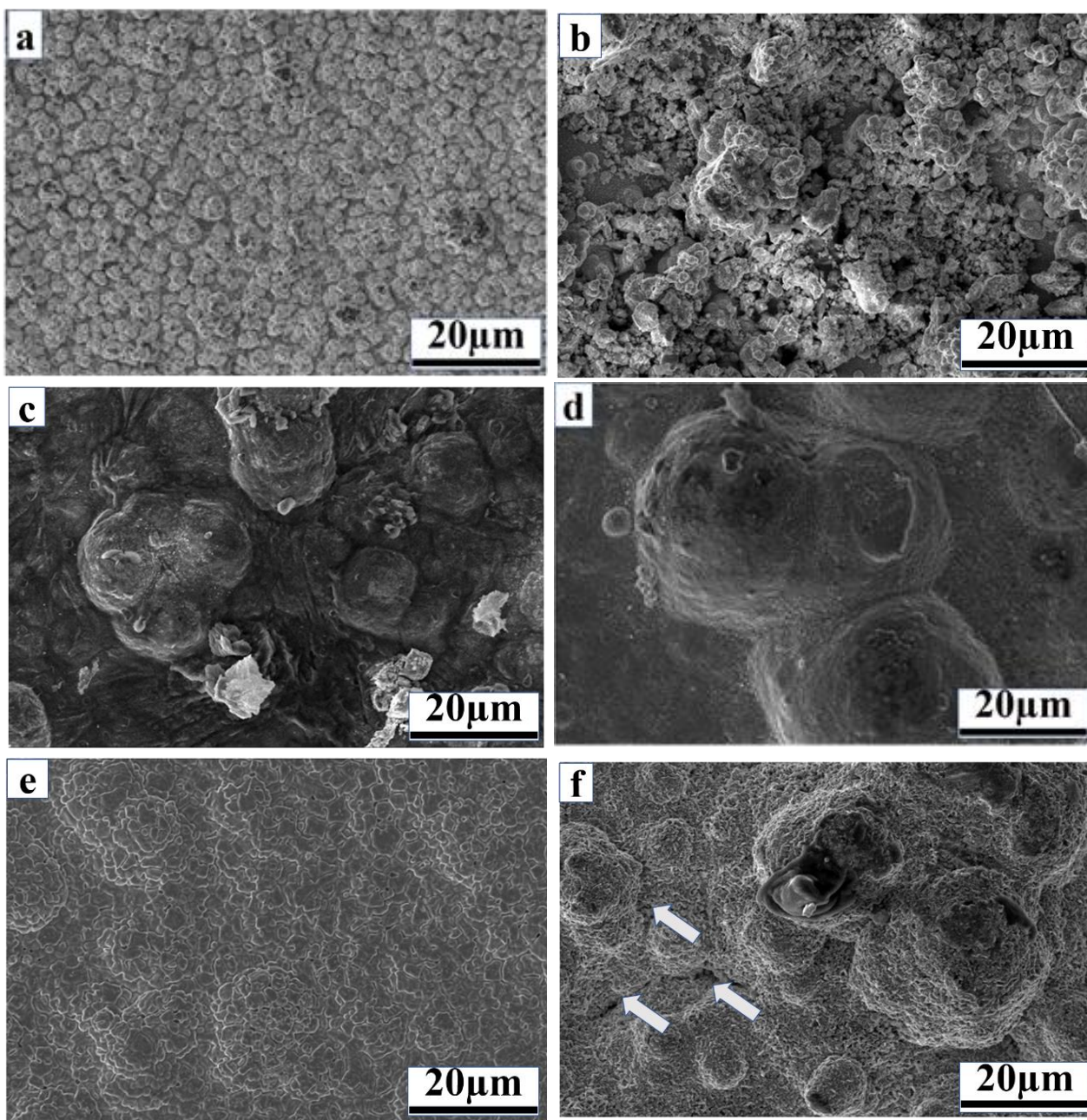


**Figure 1.** FESEM images of Coating-1: (a) as-deposited; (b) heat treated at 400 °C, 1 h; (c) heat treated at 400 °C, 4 h; (d) heat treated at 600 °C, 1 h; (e) heat treated at 600 °C, 4 h; (f) heat treated at 800 °C, 1 h

This implies a change from Ni-P to Ni-Cu-P layer or *vice versa*. Also, the top and bottom layers almost have the same thickness. The absence of a visible demarcation between the top and the bottom layer indicates excellent adhesion and compatibility between the two layers of the deposit.

In the case of Ni-Cu-P coating, the deposition process is influenced by the incorporation of Cu due to the redox potential difference between Ni and Cu. Copper will be deposited first and foremost. The addition of Cu to a binary Ni-P alloy coating improves the crystallinity of the coating [36]. The copper content of the Ni-Cu-P layer remains around 9-10 % for both deposits. The cross-section of the coating shows the absence of porosity and other defects. This implies that the coating is expected to possess good corrosion resistance.

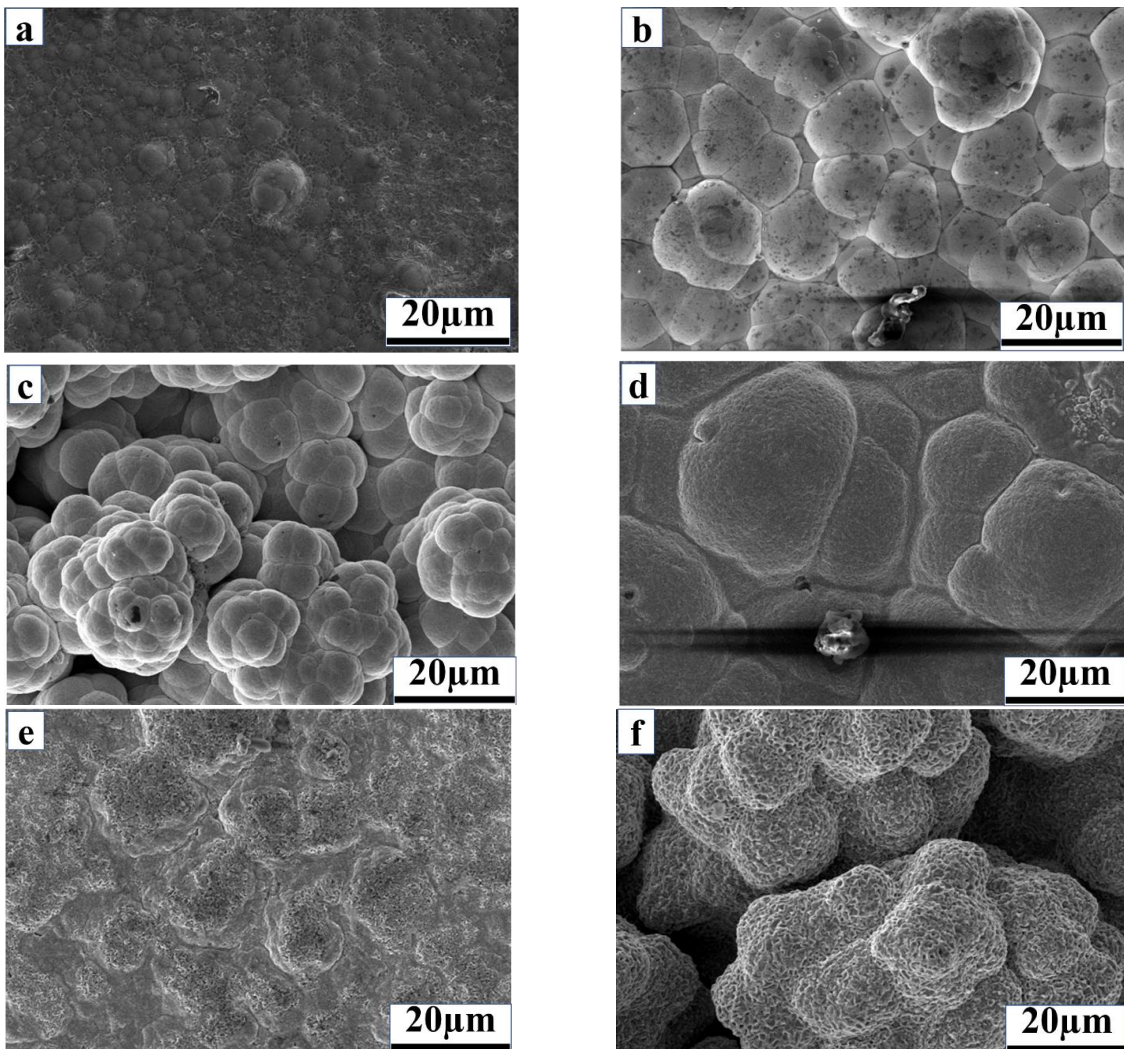


**Figure 2.** FESEM images of Coating-2: (a) as-deposited; (b) heat treated at 400 °C, 1 h; (c) heat treated at 400 °C, 4 h; (d) heat treated at 600 °C, 1 h; (e) heat treated at 600 °C, 4 h; (f) heat treated at 800 °C, 1 h

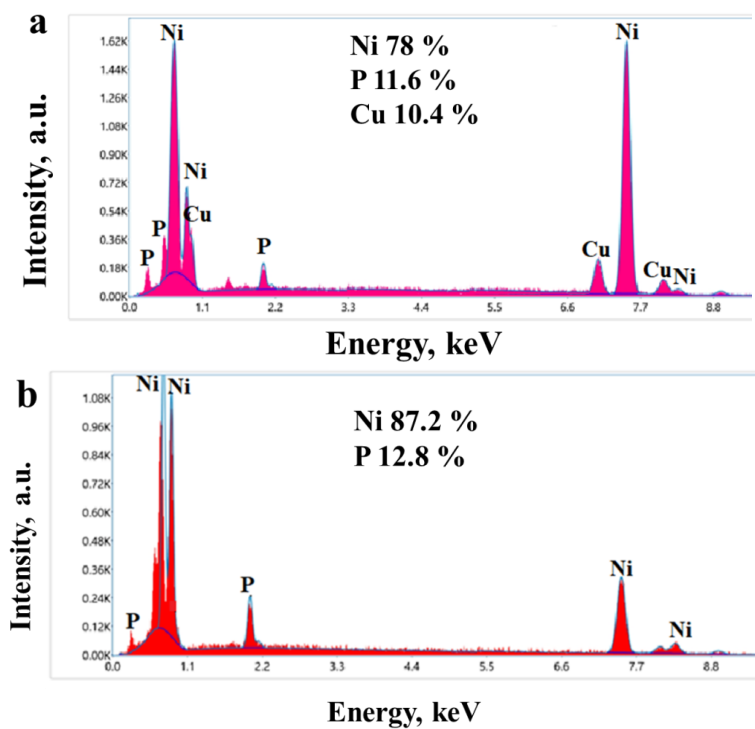


**Figure 3.** EDX spectra of (a) Coating-1 and (b) Coating-2

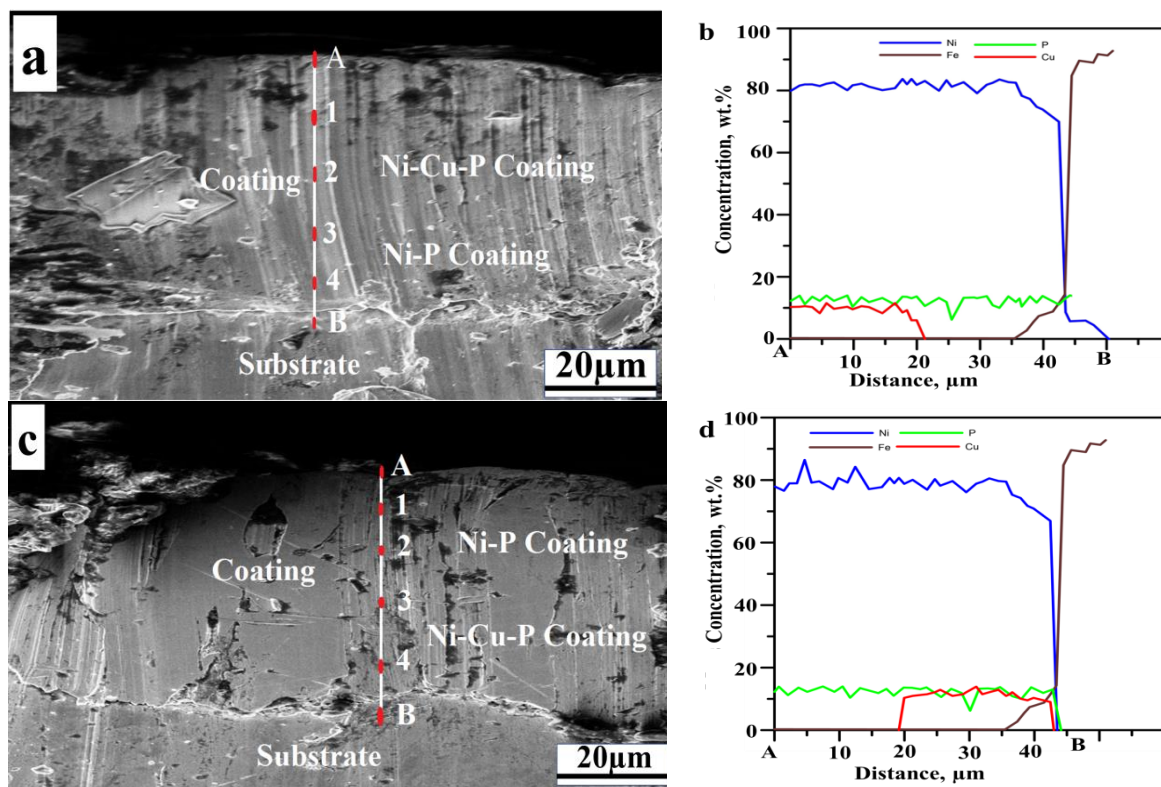


**Figure 4.** Coating cross-section showing line EDX results of: (a, b) Coating-1 and (c, d) Coating-2

### Phase structure

Figure 5 depicts the XRD analysis of both the duplex Coating-1 and Coating-2. The as-deposited coating has a broad peak, implying that it is amorphous. The single broad peak implying Ni (111) plane is observed at a diffraction angle ( $2\theta$ ) between  $40\text{--}50^\circ$ . As no significant change is noticed in the phase structure for the sample heat-treated at  $200^\circ\text{C}$ , the corresponding XRD plot is not presented. For heat treatment at temperatures of  $400^\circ\text{C}$  and above, the coating displays many crystalline peaks, mostly nickel phosphide ( $\text{Ni}_3\text{P}$ ) phases in (321), (112), (141), and (322) planes. At  $400^\circ\text{C}$  temperature, due to the higher diffusivity of Cu, it enters into the Ni lattice to form NiCu. Because of the larger atomic radius of Cu than Ni, the dissolution of copper in the nickel lattice increases the size of the lattice structure. At high temperatures, dark cupric oxide ( $\text{CuO}$ ) is obtained. Furthermore, at high temperatures (at  $600$  or  $800^\circ\text{C}$ ) and 1 and 4 h duration, a variety of oxides with Ni and Cu have been detected. Apart from these, a few hard and brittle crystalline copper phosphide ( $\text{Cu}_3\text{P}$ ) phase is obtained. The formation of the phosphides  $\text{Ni}_3\text{P}$ , in particular, is expected to enhance the hardness of the primary reason for these oxide formations is the entrapped air within the furnace. At high temperatures, there is also an increase in peak intensity and sharpening, visible at  $600$  and  $800^\circ\text{C}$  for 1 h duration. Grain refining at higher temperatures shows increased peak intensity in the XRD plot. A metastable  $\text{Ni}_8\text{P}_3$  phase is obtained at high temperatures for the Ni-Cu-P as the outer layer of deposition.

For Coating-2, the precipitation of phases is almost similar to Coating-1. It is interesting to note the presence of  $\text{Cu}_3\text{P}$  as one of the phases considering the top layer being Ni-P. This may be explained by the fact that Cu ion may have travelled near the surface of the coating by diffusion and when the sample is exposed to high temperatures in the furnace. At  $800^\circ\text{C}$  temperature and 4 h duration, dark NiO phase is obtained.

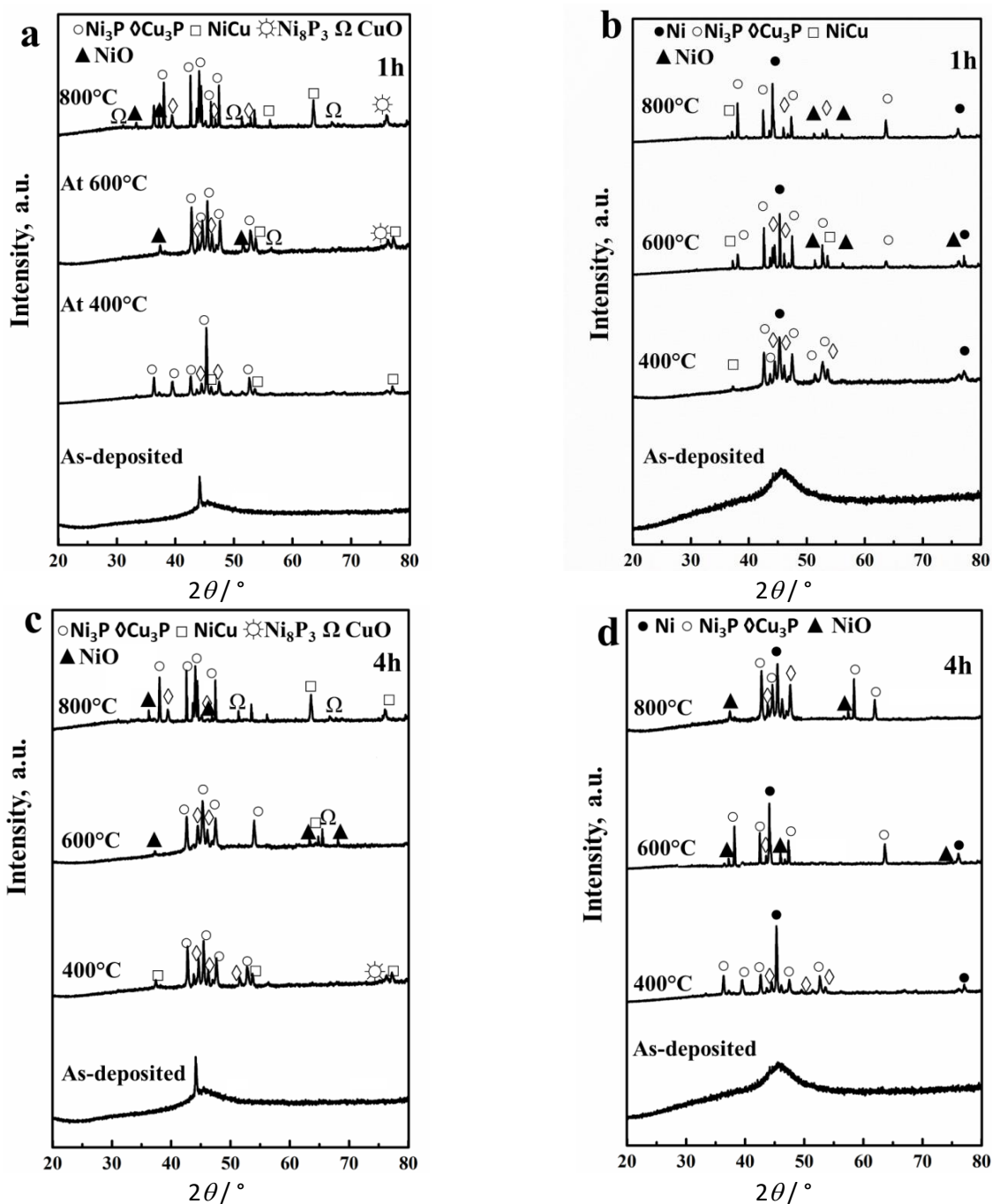


Figure 5. XRD plots of: (a) Coating-1, 1 h; (b) Coating-2, 1 h; (c) Coating-1, 4 h; (d) Coating-2, 4 h

### Microhardness of duplex coating

The microhardness of the present duplex coating is displayed in Figure 6. For Coating-1, the microhardness value is 568 HV<sub>0.1</sub> in the as-deposited coating. To improve the microhardness value, the coating was heat treated in various temperature range from 200 to 800 °C and time durations of 1 and 4 h.

At 200 °C heat treatment temperature, minimal change is observed due to lesser microstructure change. The higher hardness of duplex electroless nickel coatings is attributed to both solid solutions strengthening and precipitation hardening during heat treatment (above phase transition temperature). The maximum microhardness is obtained at 400 °C heat treatment temperature and 1 h duration mainly due to the formation of hard nickel phosphide (Ni<sub>3</sub>P) along with copper phosphide (Cu<sub>3</sub>P) phases. The hardness value is increased by around 92 % compared to as-deposited coating.

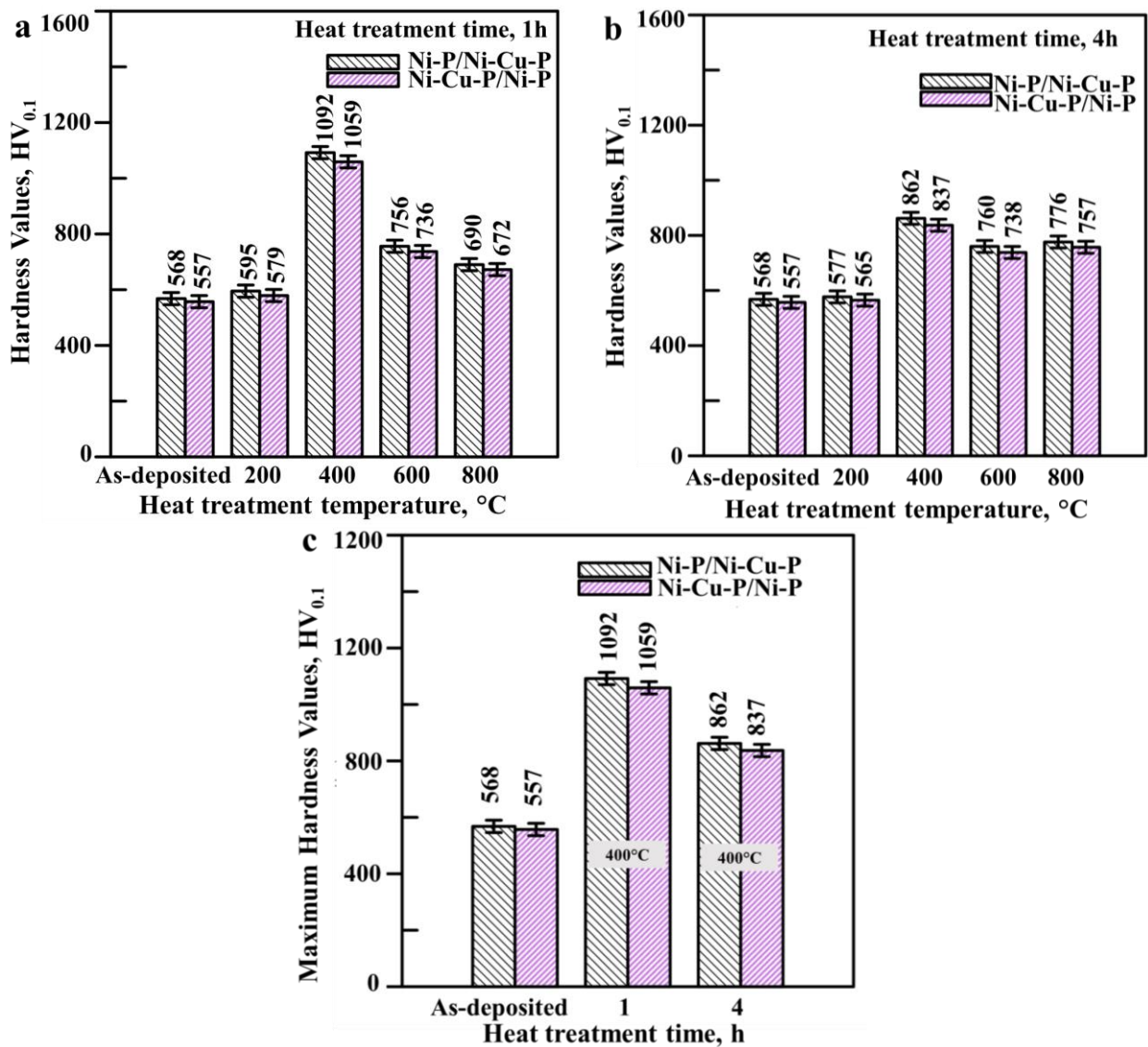


Figure 6. Hardness plots for heat treatment temperature of 200–800 °C for: (a) 1 h; (b) 4 h; (c) maximum hardness value plot

When the heat treatment duration was increased from 1 to 4 h at 400 °C temperature, the microhardness value was reduced by around 21 %, which may be due to grain coarsening. Above 400 °C temperature, the microhardness value falls mainly due to grain coarsening. However, the increased porosity of the coating may also be responsible for this decrease in the hardness of the coating. It is noted that if the porosity in the materials is increased, the load-bearing area decreases [37]. The chances for crack nucleation increase due to an increase in the subsurface porosity of the coating. This causes the weakening of the duplex coating and a decrease in its strength. Furthermore, the significant fall in P concentration when heat treated at high temperatures may also be contributing to a loss in microhardness. Finally, oxide formation at higher temperatures, like NiO and CuO, is relatively soft and dispersed over the coating surface, which is also responsible for lowering the hardness. In the case of Coating-2 (Ni-P as an outer layer of deposition), the hardness value is obtained at 557 HV<sub>0.1</sub> in the as-deposited coating. The maximum microhardness value is obtained at 400 °C temperature and 1 h duration. The hardness value is increased by around 90 % from as-deposited coating due to the formation of the hard phase. The similar trend in hardness changes with heat treatment temperature indicates the same underlying mechanisms influencing hardness as discussed for Coating-1. Overall, it can be said that heat treatment definitely increases the hardness of the

coating. However, heat treatment at higher temperatures and longer duration is not beneficial for the hardness of both coating systems. In the current investigation, the hardness of Ni-Cu-P as an outer layer is higher than that of Ni-P as the outer layer of coating from all aspects.

### Friction performance

The average coefficient of friction (COF) of both duplex coatings is shown in Figure 7 for different heat-treated states. The first thing to note is that the COF of as-deposited coating is higher than the heat-treated coatings. In fact, COF is reduced by half upon heat treatment. The heat-treated coatings display more or less a stable COF value ranging between 0.14 and 0.22, considering both coating systems. For 4 h duration heat treatment, COF ranges between 0.12 and 0.28, which is also fairly stable. The decrease in COF value post-heat treatment is mainly due to the gain in hardness of the coatings. However, some variation in the COF is also because of the formation of various phases on the coating surface, including oxides.

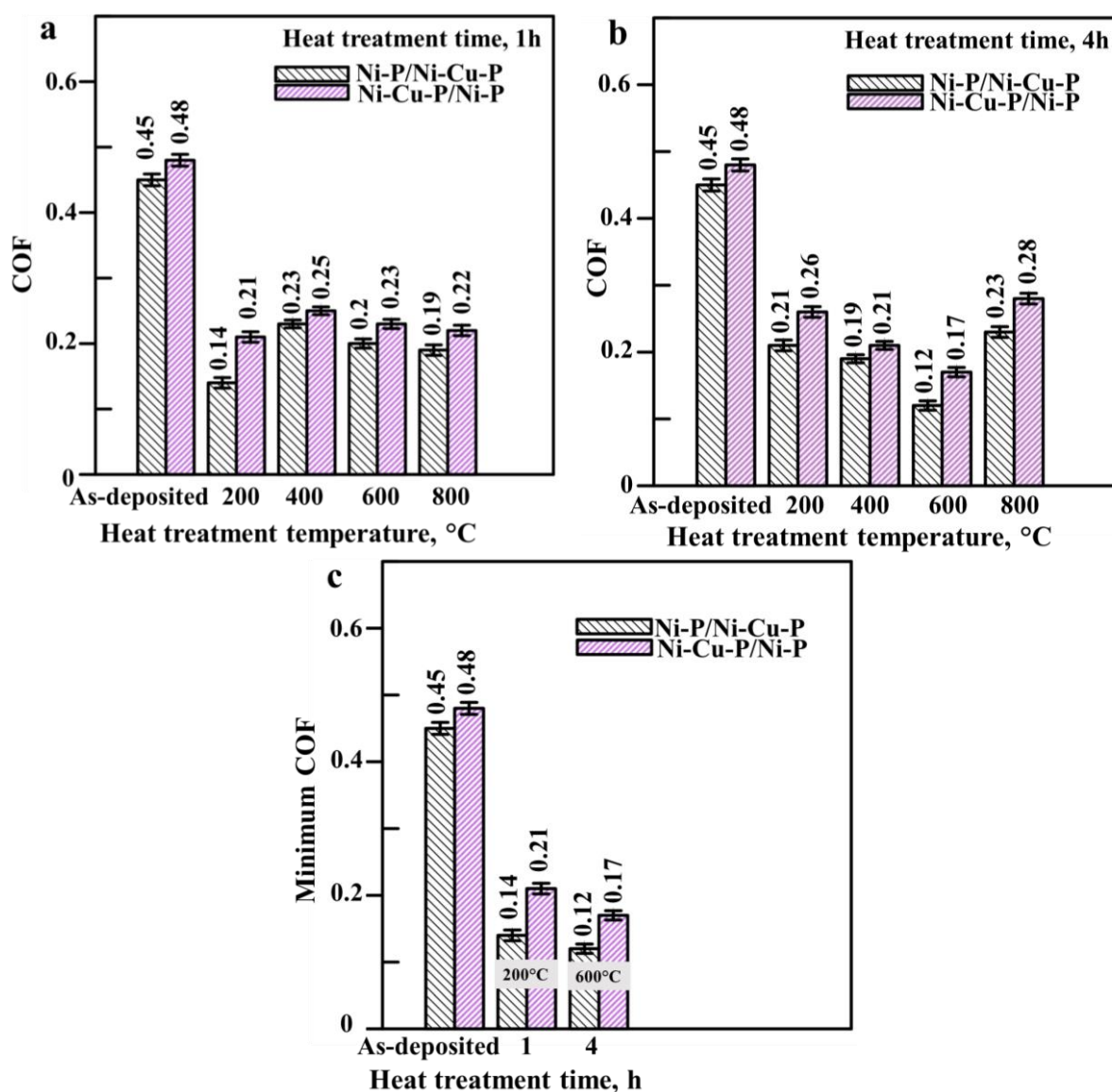


**Figure 7.** Coefficient of friction plots for heat treatment temperature of 200–800 °C: (a) 1h; (b) 4 h; (c) minimum coefficient of friction plot

The COF vs. time plots shown in Figure 8 also show quite stable friction behaviour of the current coatings. Some variation is noticed, especially for 4 h duration heat-treated samples with Ni-P as the

outer layer, which may be testimony to the fact that due to phenomena *viz.* oxide formation and grain coarsening, the integrity of the top layer is somewhat lost, which is not the case for coating with Ni-Cu-P as the top layer. Overall, it can be said that Coating-1 displays relatively lower COF compared to Coating-2.

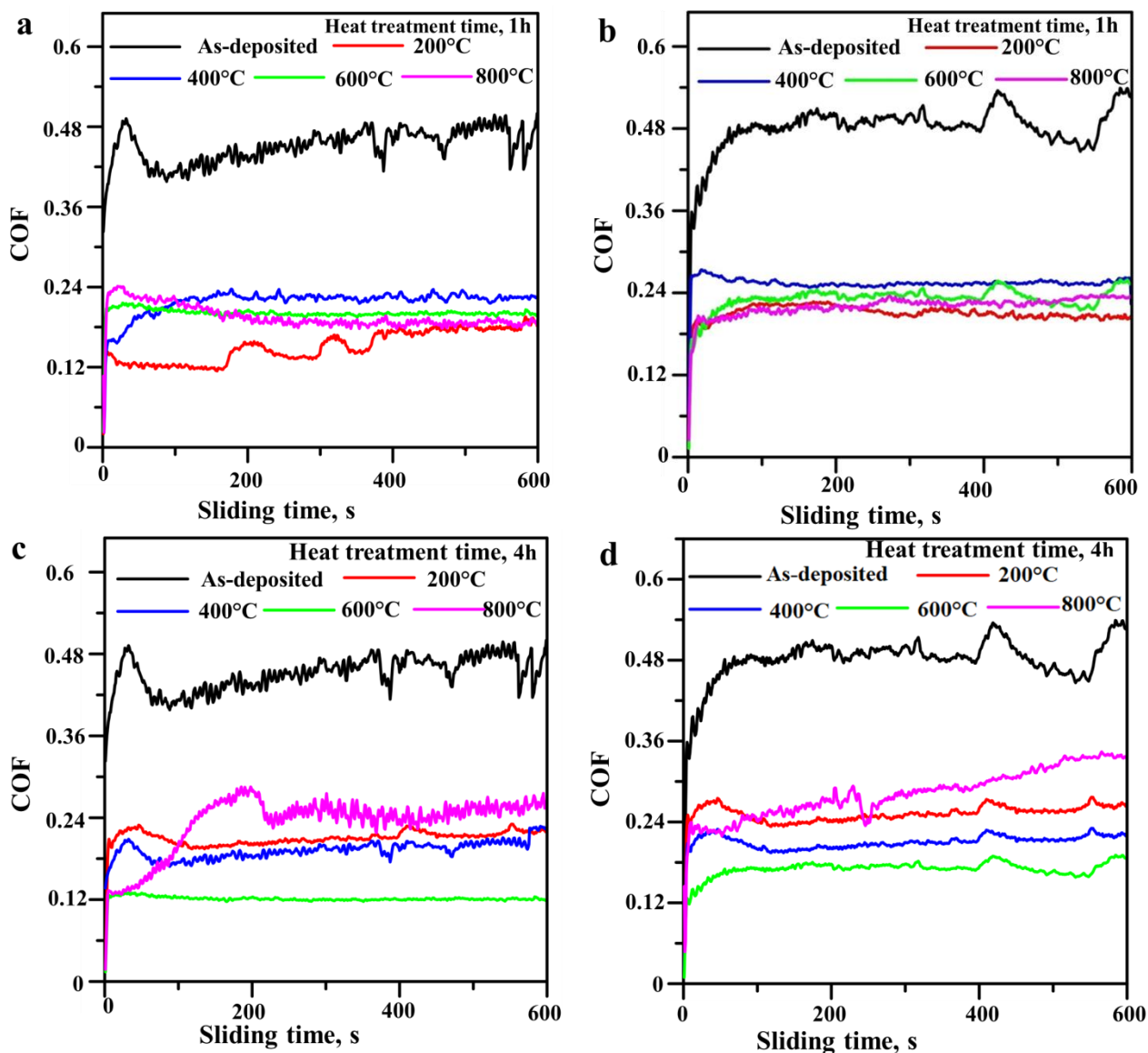


**Figure 8.** COF vs. sliding duration plots of: (a) Coating-1, 1 h; (b) Coating-2, 1 h; (c) Coating-1, 4 h; (d) Coating-2, 4 h

*Wear behavior*

The wear behavior of duplex coatings is shown in Figure 9. The first thing to note is that heat treatment definitely lowers the wear rate of as-deposited coatings. The lowest wear rate is observed for the heat treatment state of 400 °C, beyond which the wear rate increases. In fact, a very good correlation is observed between the hardness and wear results. The samples displaying higher hardness show a lower wear rates or higher wear resistance. The wear rate is reduced with heat treatment temperature due to the formation of the hard Ni<sub>3</sub>P and Cu<sub>3</sub>P phases. The minimum wear rate is obtained at 400 °C heat treatment temperature with an hour duration due to higher micro-hardness. The wear rate is reduced by around 38% as compared to as-deposited coating. At high temperatures (600 or 800°C) and longer time duration, the wear performance of the coating

degrades due to spallation and delamination of the coating. At this temperature, the wear rate increases due to the formation of oxides, viz. NiO and CuO. This oxide layer is normally unwanted. This oxide layer has lower shear strength and presents poor adhesion to the interlayer of duplex coatings, tending to cause delamination of the top layer. Porosity encountered at higher temperatures and longer duration heat treatment may also affect the wear behavior of the coatings, as seen in Fig. 9b. This is also reported in one of the previous studies [38]. In fact, the wear performance of coatings heat treated at 800°C is almost the same as as-deposited coatings. Another significant observation is that among both the coating systems, coating with Ni-Cu-P as the outer layer exhibits a lower wear rate. This is due to the higher hardness of the Ni-Cu-P layer, as already seen in the hardness study. However, for both coatings, the minimum wear rate is observed at 400 °C heat treatment temperature as shown in Figure 9c. In both types of coatings, similar wear behavior is observed. Duplex coating with Ni-Cu-P as the outer layer displays the best wear performance in all aspects.

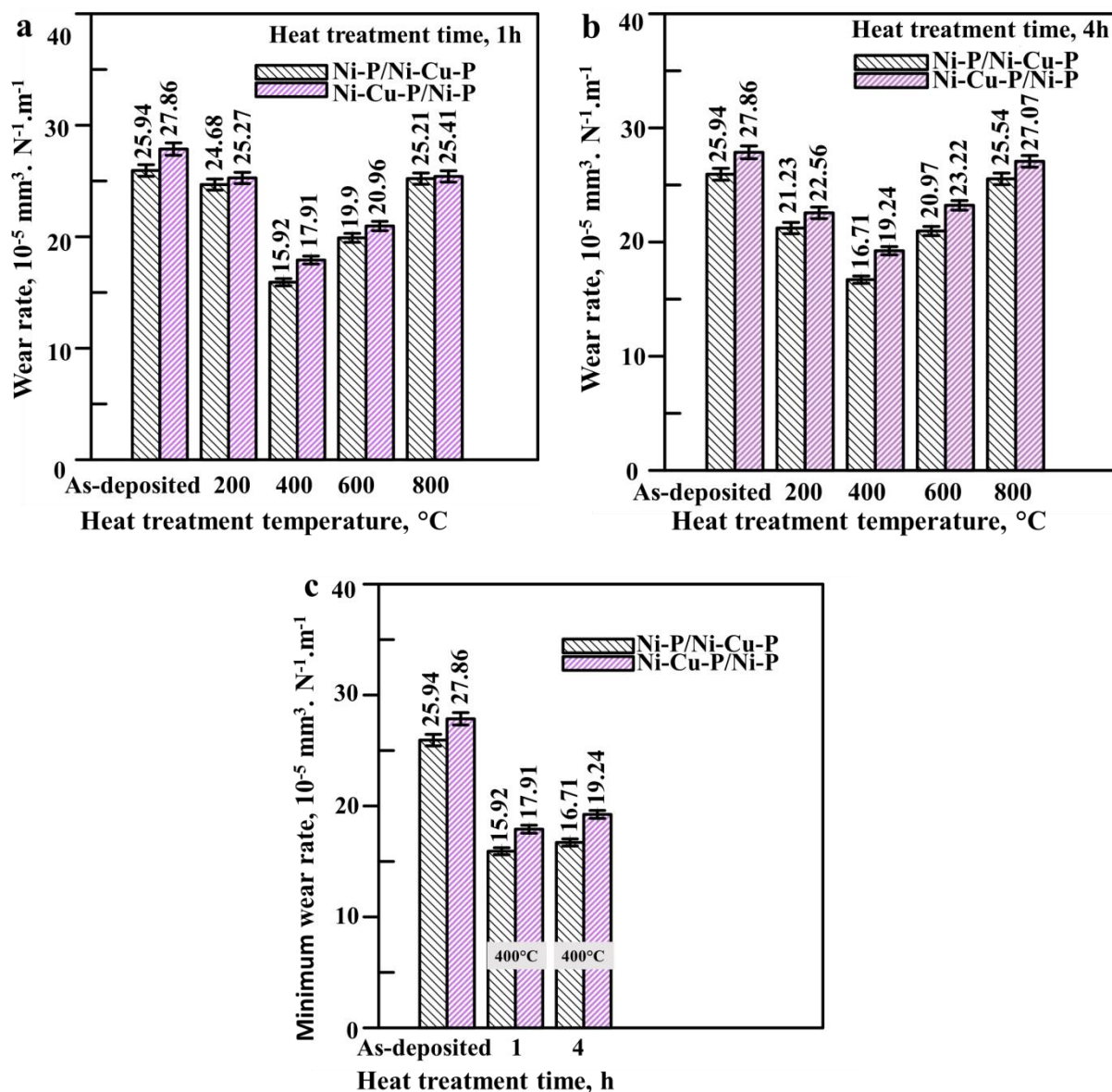


**Figure 9.** Wear rate for heat treatment temperature of 200–800 °C for: (a) 1 h; (b) 4 h; (c) minimum wear rate

#### Wear mechanism

The detailed wear mechanism is studied with the help of SEM and EDX of the wear-tested samples presented in Figures 10 to 14.

The wear behavior of Coating-1 in an as-deposited state is shown in Figure 10a. The worn surface morphology of the as-deposited coating shows ploughing due to sliding under the applied load. Ploughing marks are shown by white arrows, indicating the occurrence of an abrasive wear mechanism [39,40]. Some pits and prows are also observed, indicating that adhesive wear might have occurred. The presence of Fe in the EDX plot (Figure 10b), however, confirms the occurrence of adhesive wear. This is because the only possible source of Fe is the ferrous counterface (material against which the sample is rubbed during the test) and this exchange occurs due to the high mutual solubility of iron and nickel. A small amount of oxygen is also detected in the sample showing oxidation at the sliding interface.

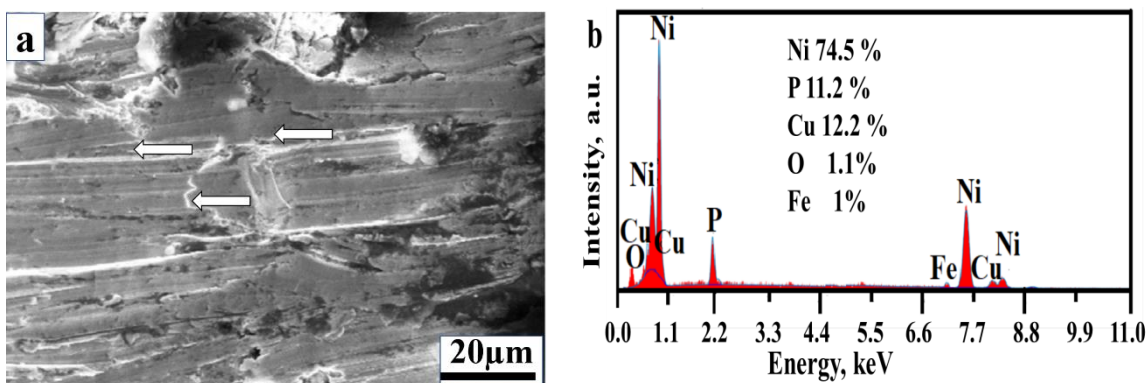


Figure 10. Worn surface of as-deposited Coating-1: (a) SEM image; (b) EDX plot

For 400 °C, 1h treated sample (Figure 11a), the worn surface exhibits plastic deformation due to sliding under the applied load. Abrasion marks in the sliding direction are also present. Few deep grooves and micro-cracks are also observed on the surface of the coated sample. This indicates a mixture of adhesive and abrasive wear mechanisms. For 600 °C, 1 h treated sample (Figure 11b), some spallation of the coating is observed apart from the presence of abrasive marks.

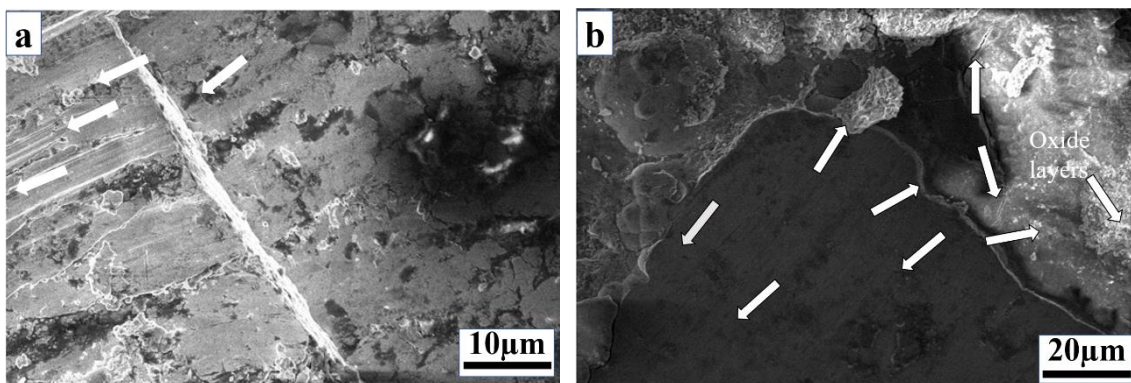
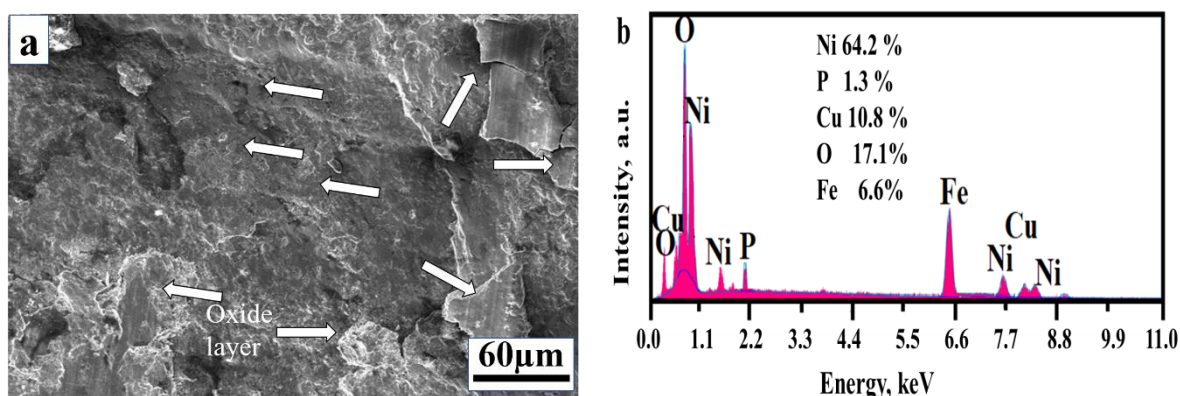


Figure 11. SEM images of worn surface of Coating-1 heat treated at: (a) 400°C, 1h; (b) 600°C, 1h.

For the 800 °C, 4 h sample (Figure 12a), the tested surface shows significant damage in spallation, delamination, cracking, etc., while abrasive marks are not visible. This implies that the abrasive wear mechanism is not the governing mechanism. Rather, the wear behavior of the sample is impacted by the formation of an oxide layer on its surface. This is supported by the EDX results, where about 17.1 % oxygen is detected on the tested surface (Figure 12b).



**Figure 12.** Worn surface of Coating-1 heat treated at 800°C, 4 h: (a) SEM image and (b) EDX plot

The results of wear-tested samples of Coating-2 are shown in Figures 13 and 14. The as-deposited sample (Figure 13a) shows abrasion marks (indicated by white arrows) along the sliding direction. Besides, there is much pressed wear debris almost welded to the surface. This indicates the occurrence of 3-body abrasion. It is interesting to see the presence of Cu in the EDX results (Figure 13b), as the coating under consideration has Ni-P in the outer layer. Now, discreet cuts and damages are observed on the coating surface, through which Cu from the bottom layer might have been detected. Adhesive wear also occurs, which is supported by the presence of pits and prows as well as the detection of Fe.

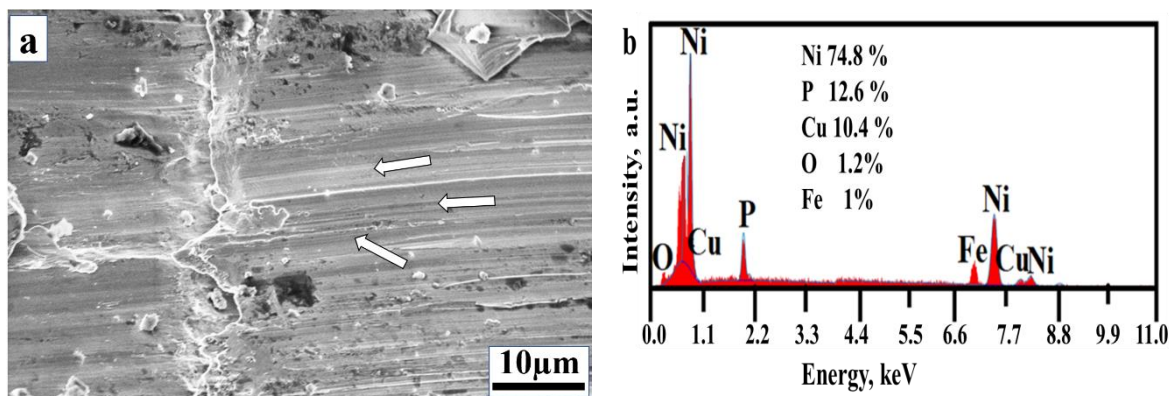


**Figure 13.** Worn surface of as-deposited Coating-2: (a) SEM image; (b) EDX plot

For the sample heat-treated at 400 °C, 1 h (Figure 14a), the worn surface exhibits the abrasion marks along with the smeared wear debris patches.

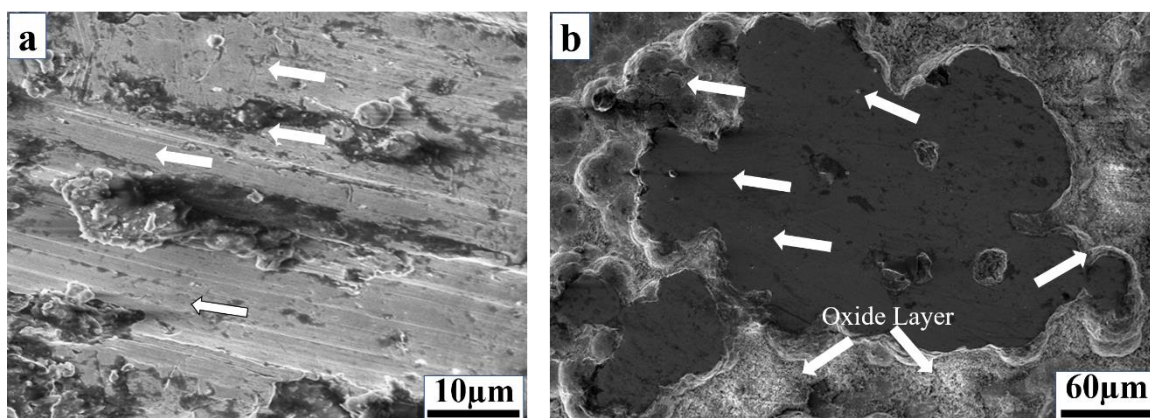


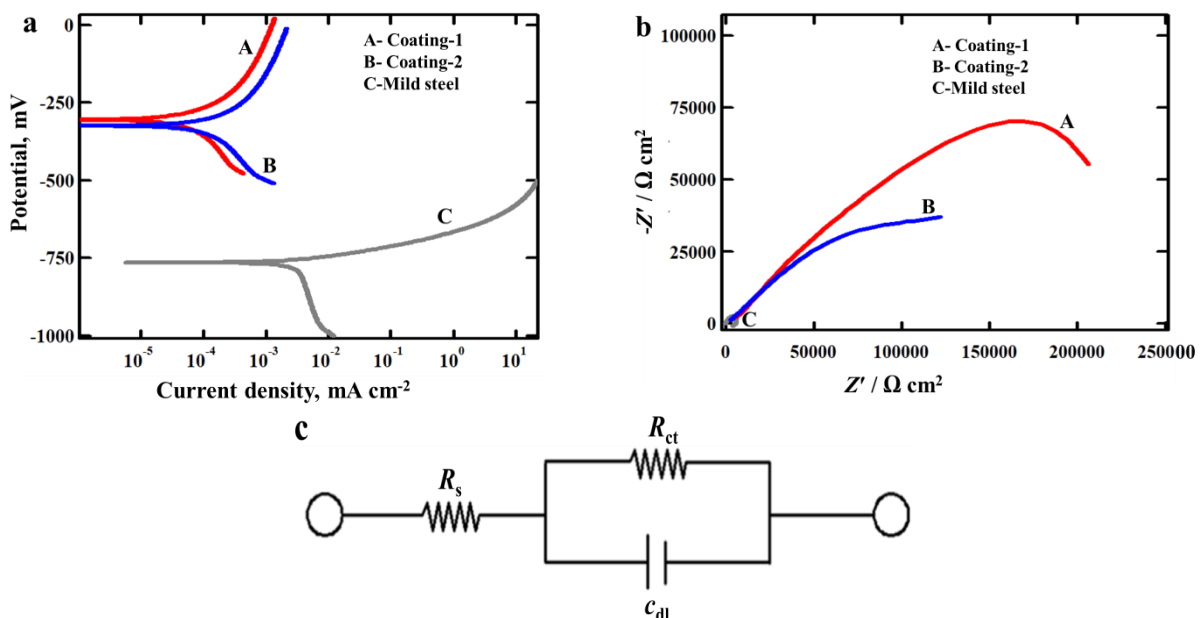
**Figure 14.** SEM image of worn surface of Coating-2 heat treated at: (a) 400 °C, 1 h; (b) 600 °C, 1 h

However, for the sample heat-treated at 600 °C, 1 h, some spallation of the coating is again due to the formation of oxides on the top surface. As the worn surface of Coating-2 depicts features almost similar to Coating-1, it may be concluded that similar types of wear mechanisms are underlying both duplex coating systems. Hence, further discussion in this regard for Coating-2 is not presented.

**Corrosion behavior**

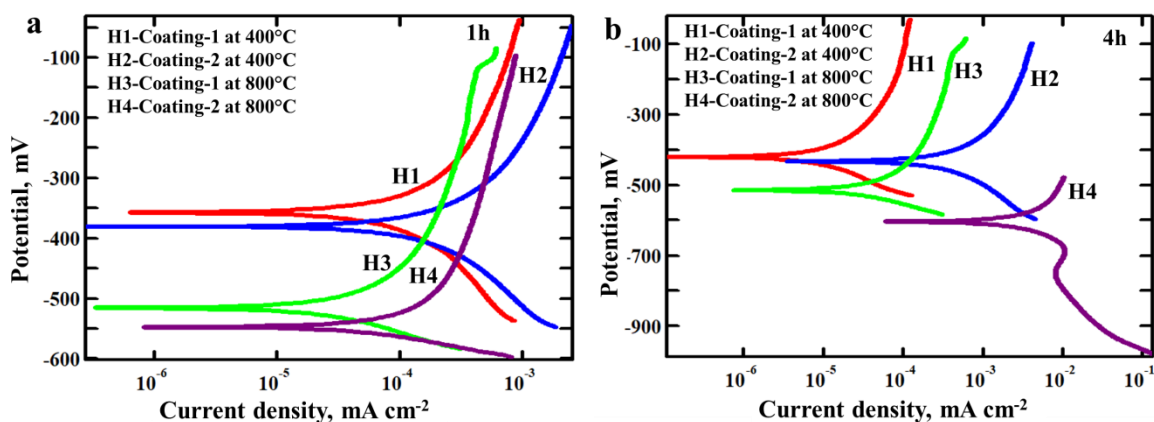
The potentiodynamic polarization performance of mild steel substrates is compared to the coated specimens in the form of Tafel plots, as presented in Figure 15a. The cathodic and anodic portions of the plots are distinctly visible for all the samples. Figure 15a shows that duplex coating has a higher corrosion potential than uncoated samples, indicating significant protection against corrosion. Again, the system with Ni-Cu-P as the outer layer of deposition (Coating-1) displays a passivation phase in the polarization curve, as was also reported by Chen *et al.* [41]. This leads to the conclusion that the performance of Coating-1 is relatively better compared to the system with Ni-P as the outer layer (Coating-2). Generally, it has been demonstrated that the presence of P can raise  $E_{corr}$  and decrease  $j_{corr}$  in Ni-P coatings and their variations by boosting anodic and cathodic processes and accelerating Ni dissolution. The present duplex coating achieves a significant reduction of  $j_{corr}$ . Moreover, the presence of Cu inhibits the corrosion process in Ni-P, as Cu has a higher reduction potential than Ni [42].

The impedance results of mild steel are also compared to its coated counterparts in the form of Nyquist plots, as presented in Figure 15b. The assumed circuit is a simple Randles circuit, as illustrated in Figure 15c, where  $R_s$ ,  $R_{ct}$  and  $C_{dl}$  refer to solution resistance, charge transfer resistance due to corrosion, and interfacial double-layer capacitance, respectively. Nyquist plot of this combination would present a semicircle response with the diameter determined by the value of charge transfer resistance,  $R_{ct}$ . Higher diameters of Nyquist plots shown in Figure 15a for duplex coatings compared to the mild steel substrate suggest better corrosion protection provided by the coatings. This implies an increase in impedance magnitude and, thus, enhanced resistance against corrosion. The higher corrosion resistance of Coating-1 compared to Coating-2 is also evident from the plots. The actual values of the corrosion parameters, as determined from the tests, are listed in Table 4.



**Figure 15.** (a) Polarization plots; (b) Nyquist plots; (c) equivalent circuit diagram for steel and coated samples

The effect of heat treatment conditions on the corrosion behaviour of the coatings is also studied and presented in Figures 16 and 17. The Tafel polarization plots of heat-treated samples are displayed in Figure 16. The potentiodynamic polarization results show that, in general, the corrosion potential moves towards a more negative region after heat treatment. This indicates a loss in corrosion resistance after heat treatment. This is quite understandable as the amorphous structure in as-deposited coating turns crystalline after heat treatment, and their grain boundaries act as active sites for attack by corrosive media [41]. It is interesting to find that the  $E_{\text{corr}}$  value of the duplex coating is reduced and  $j_{\text{corr}}$  value increases with increasing heat treatment temperature and time duration (Table 4). This implies that crystallinity is not the only factor impacting the corrosion resistance of the present coatings after heat treatment. The passivation phenomenon observed for the as-deposited systems seems to be weakened due to heat treatment [41]. Moreover, at higher temperatures, due to grain coarsening and higher stresses, there is visible cracking on the surface of the coating, as observed previously. Through these damages and microcracks,  $\text{Cl}^-$  ions can enter and the corrosion resistance of the coatings is compromised. Moreover, the formation of oxide phases at these heat treatment conditions also presents a heterogeneous surface having local variation in corrosion potential leading to an intense attack by NaCl solution.

**Figure 16.** Polarization plots for heat-treated samples: (a) 1h duration; (b) 4h duration**Table 4.** Corrosion data obtained from Tafel extrapolation and Nyquist plots.

Sample	$E_{\text{corr}} / \text{mV}$	$j_{\text{corr}} / \mu\text{A cm}^{-2}$	$R_{\text{ct}} / \text{k}\Omega \text{ cm}^2$	$C_{\text{dl}} / \mu\text{F cm}^{-2}$
Mild steel	-764	0.4619	7.94	18.76
Coating-1, as-deposited	-302	0.0183	265.0	3.541
Coating-2, as-deposited	-323	0.0211	189.0	5.018
Coating-1, at 400 °C 1 h	-358	0.0277	920.3	4.901
Coating-2, at 400 °C 1 h	-382	0.0684	478.0	10.29
Coating-1, at 800 °C 1 h	-514	0.0342	320.5	1.075
Coating-2, at 800 °C 1 h	-545	0.0228	140.3	2.354
Coating-1, at 400 °C 4 h	-420	0.0164	3802.0	1.353
Coating-2, at 400 °C 4 h	-432	0.0152	850.2	18.57
Coating-1, at 800 °C 4 h	-548	0.0221	314.0	2.659
Coating-2, at 800 °C 4 h	-607	0.0980	106.2	6.477

Nyquist plots for the heat-treated coatings are shown in Figure 17. Almost similar patterns are observed for all samples. However, the curves vary in size. This implies that the same underlying mechanism acts over a different effective area. Similar reporting has been made by earlier studies [5].

Coating-1, in general, displays higher impedance values compared to Coating-2 (Table 4). As already discussed, this is because Coating-1 has Ni-Cu-P as the outer layer, which is reported to have higher corrosion resistance ability than Ni-P coatings. Coating-1 heat treated at 400 °C, 4h has the largest diameter (in Nyquist plot), which indicates its highest resistance against corrosion. This is followed by Coating-1 heat treated at 400 °C, 1h. Both the coatings, when heat treated at 800 °C, display lower impedance values compared to samples treated at 400 °C. This implies that corrosion resistance is compromised at higher heat treatment temperatures. In fact, at 800 °C oxide formation occurs on the coating surface and micro-cracks are generated, as seen from the microstructural studies. The duration of heat treatment induces a different impact on the corrosion behaviour of the coating at different heat treatment temperatures. At 400 °C, the increased duration of heat treatment resulted in increased corrosion resistance. However, for 800 °C, the corrosion resistance decreases with the increased duration of heat treatment. This may be due to the increased thermal stress related manifestations on the coating surface at these conditions apart from the oxide and crack formation. 800 °C, 4h heat treatment condition results in the lowest corrosion resistance among the coated samples, but still, the same is better than the base substrate. This implies the coating is still able to provide protection to the steel substrate. In general, EIS and potentiodynamic polarization findings are consistent. Overall, duplex electroless Ni-P/Ni-Cu-P coatings (Coating-1) have the highest corrosion resistance both in the as-deposited and heat-treated states.

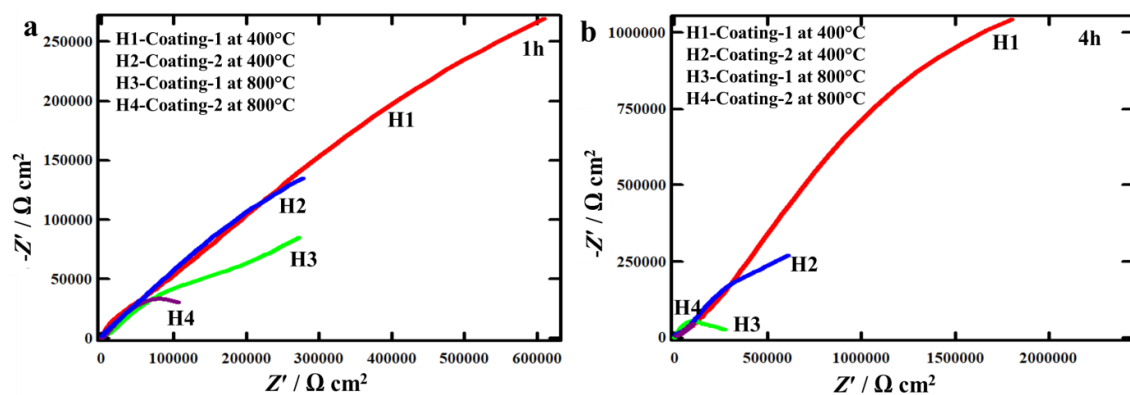


Figure 17. Nyquist plots for heat-treated samples: (a) 1 h duration; (b) 4 h duration

From the present study, it is seen that duplex Ni-P/Ni-Cu-P is a promising coating for surface protection. Particularly the system with Ni-Cu-P as the outer layer displays higher wear resistance which improves further after heat treatment due to the phase transformation of the coating and precipitation of harder phases. The as-deposited coating is able to give good protection to the substrate surface against corrosion due to the former's amorphous structure and ability to generate a passive film. In fact, Cu inhibits, to some extent, the crystalline transformation of the coating during heat treatment and results in enhanced corrosion resistance. Apart from this, Cu aids in the formation of the passive film. After heat treatment, the corrosion resistance ability of the coating increases in general. Heat treatment at 400 °C results in the highest corrosion resistance. However, heat treatment beyond 400 °C seems to have a negative impact on the coating, considering both the wear and corrosion resistance. Oxide formation, and generation of cracks and pores leads to a significant lowering of the wear and corrosion resistance of the present duplex coatings.

## Conclusions

Duplex electroless deposited Ni-P/Ni-Cu-P coatings are found to enhance the surface hardness of mild steel substrates. Heat treatment further increases the hardness of the coatings due to the

precipitation of harder phosphide phases. Heat treatment at higher temperatures viz. 600 and 800 °C results in grain coarsening and oxide formation, leading to a lowering of the gained hardness. The following conclusions may be drawn from the study:

- The duplex coatings display a consistent friction behaviour. Post-heat treatment, the wear resistance of the coating improves significantly as a result of the increase in the hardness of the coating.
- The corrosion study shows that the duplex coatings are able to provide significant protection to the mild steel substrates. Heat treatment results in an increase in the corrosion resistance of the coatings.
- Corrosion resistance is severely compromised for higher heat treatment conditions, viz. 800 °C This is due to the formation of microcracks and oxides at these conditions.

Overall, it can be said that 400 °C and a time duration of 1 h is the optimal condition of heat treatment for the present duplex coatings. Beyond this temperature, the tribological and corrosion performance of the coatings are severely affected. The duplex combination with Ni-Cu-P as the top layer performs better in almost all aspects compared to the coating with Ni-P as the top layer.

### Conflict of interest

The authors declare that there is no conflict of interest related to the publishing of the present work.

### References

- [1] M. Palaniappa, S. K. Seshadri, Friction and wear behavior of electroless Ni–P and Ni–W–P alloy coatings, *Wear* **265(5-6)** (2008) 735-740. <https://doi.org/10.1016/j.wear.2008.01.002>
- [2] P. Biswas, S. K. Das, P. Sahoo, Role of heat treatment on the friction and wear behavior of duplex electroless nickel deposits, *Materials Today: Proceedings*. **66(9)** (2022) 3902-3909 <https://doi.org/10.1016/j.matpr.2022.06.322>
- [3] P. Sahoo, in *Woodhead Publishing Reviews: Mechanical Engineering Series, Materials and Surface Engineering: Research and Development*, J.P. Davim (Ed.), Woodhead/Elsevier, Cambridge/Oxford, UK, 2012, p. 163. <https://doi.org/10.1533/9780857096036.163>
- [4] P. Sahoo, S. K. Das, Tribology of electroless nickel coatings—a review, *Materials & Design* **32(4)** (2011) 1760-1775. <https://doi.org/10.1016/j.matdes.2010.11.013>
- [5] S. Banerjee, P. Sarkar, P. Sahoo, Improving corrosion resistance of magnesium nanocomposites by using electroless nickel coatings, *Facta Universitatis. Series: Mechanical Engineering* **20(3)** (2022) 647-663. <https://doi.org/10.22190/FUME210714068B>
- [6] F. Mindivan, H. Mindivan, Improvement of surface properties via an electroless Ni-B coating for commercial purity titanium, *BSEU Journal of Science* **6** (2019) 99-105. <https://doi.org/10.35193/bseufbd.566236>
- [7] F. Mindivan, H. Mindivan, C. Darcan, Electroless Ni-B coating of pure titanium surface for enhanced tribocorrosion performance In artificial saliva and antibacterial activity, *Tribology in Industry* **39(2)** (2017) 270-276. <https://doi.org/10.24874/ti.2017.39.02.15>
- [8] D. Pye, *Practical nitriding and ferritic nitrocarburizing*, ASM International, Materials Park, Ohio, USA, 2003.
- [9] R. C. Agarwala, V. Agarwala, Electroless alloy/composite coatings: A review, *Sadhana* **28(3)** (2003) 475-493. <https://doi.org/10.1007/BF02706445>
- [10] L. Li, J. Wang, J. Xiao, J. Yan, H. Fan, L. Sun, L. Xue, Z. Tang, Time-dependent corrosion behavior of electroless Ni–P coating in H<sub>2</sub>S/Cl<sup>-</sup> environment, *International Journal of Hydrogen Energy* **46(21)** (2021) 11849-11864. <https://doi.org/10.1016/j.ijhydene.2021.01.053>

- [11] H. Mindivan. Tribocorrosion behaviour of electroless Ni–P coating on AA7075 aluminum alloy, *Acta Physica Polonica A* **135** (2019) 1102-1104. <https://doi.org/10.12693/APhysPolA.135.1102>
- [12] Z. Bangwei, H. Wangyu, Z. Qinglong, Q. Xuanyuan, Properties of electroless Ni-W-P amorphous alloys, *Materials Characterization* **37(2-3)** (1996) 119-122. <https://doi.org/10.12693/APhysPolA.135.1102>
- [13] L. Wang, Y. Gao, T. Xu, Q. Xue, A comparative study on the tribological behavior of nanocrystalline nickel and cobalt coatings correlated with grain size and phase structure, *Materials Chemistry and Physics* **99(1)** (2006) 96-103. <https://doi.org/10.1016/j.matchemphys.2005.10.014>
- [14] W. Y. Chen, S. K. Tien, F. B. Wu, J. G. Duh, Crystallization behaviors and microhardness of sputtered Ni–P, Ni–P–Cr and Ni–P–W deposits on tool steel, *Surface and Coatings Technology* **182(1)** (2004) 85-91. [https://doi.org/10.1016/S0257-8972\(03\)00851-X](https://doi.org/10.1016/S0257-8972(03)00851-X)
- [15] J. Li, C. Sun, M. Roostaei, M. Mahmoudi, V. Fattahpour, H. Zeng, J. L. Luo, Characterization and corrosion behavior of electroless Ni-Mo-P/Ni-P composite coating in CO<sub>2</sub>/H<sub>2</sub>S/Cl<sup>-</sup> brine: Effects of Mo addition and heat treatment, *Surface and Coatings Technology* **403** (2020) 126-416. <https://doi.org/10.1016/j.surfcoat.2020.126416>
- [16] S. Z. Ali, L. K. Abbas, A. K. Hussein, Optimization of Electroless Ni-P, Ni-Cu-P and Ni-Cu-P-TiO<sub>2</sub> Nanocomposite Coatings Microhardness using Taguchi Method, *IOP Conference Series: Materials Science and Engineering* **1094** (2021) 012168. <https://doi.org/10.1088/1757-899X/1094/1/012168>
- [17] A. A. Aal, M. S. Aly, Electroless Ni–Cu–P plating onto open cell stainless steel foam, *Applied Surface Science* **255(13-14)** (2009) 6652-6655. <https://doi.org/10.1016/j.apsusc.2009.02.073>
- [18] J. P. Davim, *Tribology of Nanocomposites*, Springer, Heidelberg, Germany, 2013. <https://doi.org/10.1007/978-3-642-33882-3>
- [19] T. S. Narayanan, K. Krishnaveni, S. K. Seshadri, Electroless Ni–P/Ni–B duplex coatings: preparation and evaluation of microhardness, wear and corrosion resistance, *Materials Chemistry and Physics* **82(3)** (2003) 771-779. [https://doi.org/10.1016/S0254-0584\(03\)00390-0](https://doi.org/10.1016/S0254-0584(03)00390-0)
- [20] X. M. Chen, G. Y. Li, J. S. Lian, Deposition of electroless Ni-P/Ni-WP duplex coatings on AZ91D magnesium alloy, *Transactions of Nonferrous Metals Society of China* **18** (2008) s323-s328. [https://doi.org/10.1016/S1003-6326\(10\)60225-7](https://doi.org/10.1016/S1003-6326(10)60225-7)
- [21] V. Vitry, E. Francq, L. Bonin, Mechanical properties of heat-treated duplex electroless nickel coatings, *Surface Engineering* **35(2)** (2019) 158-166. <https://doi.org/10.1080/02670844.2018.1463679>
- [22] F. Mindivan, H. Mindivan, The study of electroless Ni-P/Ni-B duplex coating on HVOF-sprayed martensitic stainless steel coating, *Acta Physica Polonica A* **131(1)** (2017) 64-67. <https://doi.org/10.12693/APhysPolA.131.64>
- [23] T. S. Narayanan, I. Baskaran, K. Krishnaveni, S. Parthiban, Deposition of electroless Ni–P graded coatings and evaluation of their corrosion resistance, *Surface and Coatings Technology* **200(11)** (2006) 3438-3445. <https://doi.org/10.1016/j.surfcoat.2004.10.014>
- [24] V. Vitry, L. Bonin, Formation and characterization of multilayers borohydride and hypophosphite reduced electroless nickel deposits, *Electrochimica Acta* **243** (2017) 7-17. <https://doi.org/10.1016/j.electacta.2017.04.152>
- [25] S. Kumar, T. Banerjee, D. Patel, Tribological characteristics of electroless multilayer coating: a review, *Materials Today: Proceedings* **33** (2020) 5678-5682. <https://doi.org/10.1016/j.matpr.2020.04.207>

- [26] H. Mindivan, Tribocorrosion behavior of electroless Ni-P/Ni-B duplex coating on AA7075 aluminum alloy, *Industrial Lubrication and Tribology* **71(5)** (2019) 630-635. <https://doi.org/10.1108/ILT-05-2018-0177>
- [27] J. P. Davim, *Tribology for Engineers: A practical guide*, Woodhead/Elsevier, Cambridge/Oxford, UK, 2011. <https://doi.org/10.1533/9780857091444.frontmatter>
- [28] A. Biswas, S.K. Das, P. Sahoo, Correlating tribological performance with phase transformation behavior for electroless Ni-(high) P coating, *Surface and Coatings Technology* **328** (2017) 102-114. <https://doi.org/10.1016/j.electacta.2017.04.152>
- [29] A. Biswas, S. K. Das, P. Sahoo, Oxidation issues during heat treatment and effect on the tribo-mechanical performance of electroless Ni-P-Cu deposits, *Proceedings of the Institution of Mechanical Engineers, Part L: Journal of Materials: Design and Applications* **235(7)** (2021) 1665-1685. <https://doi.org/10.1177/1464420721999823>
- [30] M. Palaniappa, S. K. Seshadri, Structural and phase transformation behavior of electroless Ni-P and Ni-W-P deposits, *Materials Science and Engineering A* **460** (2007) 638-644. <https://doi.org/10.1016/j.msea.2007.01.134>
- [31] D. B. Lewis, G. W. Marshall, Investigation into the structure of electrodeposited nickel-phosphorus alloy deposits, *Surface and Coatings Technology* **78(1-3)** (1996) 150-156. [https://doi.org/10.1016/0257-8972\(94\)02402-2](https://doi.org/10.1016/0257-8972(94)02402-2)
- [32] D. Mohanty, T. K. Barman, P. Sahoo, Characterization and corrosion study of electroless Nickel-Boron coating reinforced with alumina nanoparticles, *Materials Today: Proceedings* **19** (2019) 317-321. <https://doi.org/10.1016/j.matpr.2019.07.216>
- [33] P. Sahoo, S. Roy, Tribological behavior of electroless Ni-P, Ni-P-W and Ni-P-Cu coatings: A Comparison, *International Journal of Surface Engineering and Interdisciplinary Materials Science (IJSEIMS)* **5(1)** (2017) 1. <https://doi.org/10.4018/IJSEIMS.2017010101>
- [34] A. Biswas, S. K. Das, P. Sahoo, Effect of copper incorporation on phase transformation behavior of electroless nickel-phosphorous coating and its effect on the tribological behavior, *Proceedings of the Institution of Mechanical Engineers, Part L: Journal of Materials: Design and Applications* **235(4)** (2021) 898-916. <https://doi.org/10.1177/1464420720981602>
- [35] C. J. Chen, K. L. Lin, The deposition and crystallization behaviors of electroless Ni-Cu-P deposits, *Journal of the Electrochemical Society* **146(1)** (1999) 137. <https://doi.org/10.1149/1.1391576>
- [36] S. Duari, A. Mukhopadhyay, T. K. Barman, P. Sahoo, Investigation of friction and wear properties of electroless Ni-P-Cu coating under dry condition, *Journal of Molecular and Engineering Materials* **4(04)** (2016) 1640013. <https://doi.org/10.1142/S225123731640013X>
- [37] A. Sinha, Z. Farhat, Effect of surface porosity on tribological properties of sintered pure Al and Al 6061, *Materials Sciences and Applications* **6(06)** (2015) 549. <https://doi.org/10.4236/msa.2015.66059>
- [38] B. Dubrujeaud, M. Vardavoulis, M. Jeandin, The role of porosity in the dry sliding wear of a sintered ferrous alloy, *Wear* **174(1-2)** (1994) 155-161. [https://doi.org/10.1016/0043-1648\(94\)90097-3](https://doi.org/10.1016/0043-1648(94)90097-3)
- [39] J. P. Davim, *Wear of Advanced Materials*, Wiley, New Jersey, USA, 2012. ISBN 978-1848213524
- [40] J. P. Davim, *Wear of Composite Materials*, DE Gruyter, Berlin, Germany, 2018. <https://doi.org/10.1515/9783110352986>
- [41] J. Chen, G. Zhao, K. Matsuda, Y. Zou, Microstructure evolution and corrosion resistance of Ni-Cu-P amorphous coating during crystallization process, *Applied Surface Science* **484** (2019) 835-844. <https://doi.org/10.1016/j.apsusc.2019.04.142>

- [42] J. Chen, Y. Zou, K. Matsuda, G. Zhao, Effect of Cu addition on the microstructure, thermal stability, and corrosion resistance of Ni–P amorphous coating, *Materials Letters* **191** (2017) 214-217. <https://doi.org/10.1016/j.matlet.2016.12.059>